Geophys. Astrophys. Fluid Dynamics, 1981, Vol. 17, pp. 237–253
0309-1929/81/1704-0237 $06.50/0

Rotating Rayleigh–Taylor Instability as a Model of Sinking Events in the Ocean†

M. K. DAVEY‡

Joint Institute for the Study of the Atmosphere and Ocean, University of Washington, Seattle, WA 98195, U.S.A.

and

J. A. WHITEHEAD, Jr.

Woods Hole Oceanographic Institution, Woods Hole, MA 02543, U.S.A.

(*Received August 8, 1980*)

The development of small disturbances in a statically unstable two-layer rotating fluid is investigated. With horizontal eddy viscosity included, there is a maximum growth rate σ_{max} at some preferred wavelength L_{max}. This scale selection mechanism may determine the characteristic size of deep convection events in the ocean following a sudden cooling of the surface. Horizontal scales of 500 m or less are estimated. Unless growth rates are small ($\sigma_{max} \ll f$) the effect of the Earth's rotation on σ_{max} and L_{max} is minor.

1. INTRODUCTION

It has been known for some time that substantial mixed-layer deepening can occur during severe winter storms, with subsequent formation of deep water masses. Perhaps the clearest understanding of such events has come from observations by the MEDOC group (1969). The picture as related by Stommel (1972) is of a dramatic deepening of the mixed layer (2000 m in 10 days) over a confined region. In this region the surface density was increased by evaporation and sensible cooling to that of the deep Mediterranean water. The evidence suggests that in this case the lateral structure of the convective region was determined principally by the

†Contribution No. 9 of the Joint Institute for the Study of the Atmosphere and Ocean.

‡Present Address: Department of Applied Mathematics and Theoretical Physics, University of Cambridge, Silver Street, Cambridge CB3 9EW, U.K.

distribution of surface density just prior to and during the cold winter storm.

Deep convection events with strong local preconditioning are undoubtedly the easiest to locate and observe. However, it is by no means certain that all events have this property—there are alternative dynamical mechanisms with inherent scale and structure. One such mechanism involves the growth of a small disturbance in a rotating fluid with a density inversion, and as such is a rotating version of Rayleigh–Taylor instability. (The Rayleigh–Taylor instability problem is discussed in detail by Chandrasekhar 1961.)

Hide (1956) has developed general linear equations and a variational principle for systems with both rotational and viscous effects. Detailed results were given for the special cases of two infinitely deep layers and of exponential stratification with prescribed vertical velocity. In the following theory two layers of finite depth are used. (Note that the two-layer geometry is intended as an approximation to some smoother density profile.) Simple equations for small perturbations are obtained by neglecting vertical viscosity, and dispersion relations are derived from these in the next section.

With viscosity present density inversions are unstable for disturbances of all wavelengths. Growth rates decay to zero in the limits of very long and very short waves, and there is a maximum σ_{max} with associated wavelength L_{max}. When growth rates are small ($\sigma \gtrsim f$, where f is the Coriolis parameter), rotation effects become important for length scales L greater than or comparable to the Rossby deformation radius L_R, effectively decreasing σ_{max} and L_{max}. (In the limiting case of inviscid rotation, the system is stable for $L > L_R$).

Growth rates for a wide range of parameters are given in Section 4, and the results are discussed in Section 5. Due to the many approximations used in deriving a simple analytic theory, only order-of-magnitude estimates can be made for the oceanic application.

2. BASIC EQUATIONS AND DISPERSION RELATIONS

A system with layers of depth H_j and constant density ρ_j ($j=1,2$) will be considered (see Figure 1). Surface wave effects are neglected, so there is a flat stress-free boundary at $z=H_1$. The lower boundary at $z=-H_2$ is also flat, and the interface between the layers is at $z=\eta(x,y)$. (At rest the interface is at $z=0$.) The density difference $\Delta\rho=\rho_2-\rho_1$ is small compared to ρ_j, so the Boussinesq approximation can be used. No background flow is allowed, so the only motion is due to initially small ($\eta \ll H_j$) wavelike perturbations of the interface. As a first approximation linearised equations and boundary conditions are used.

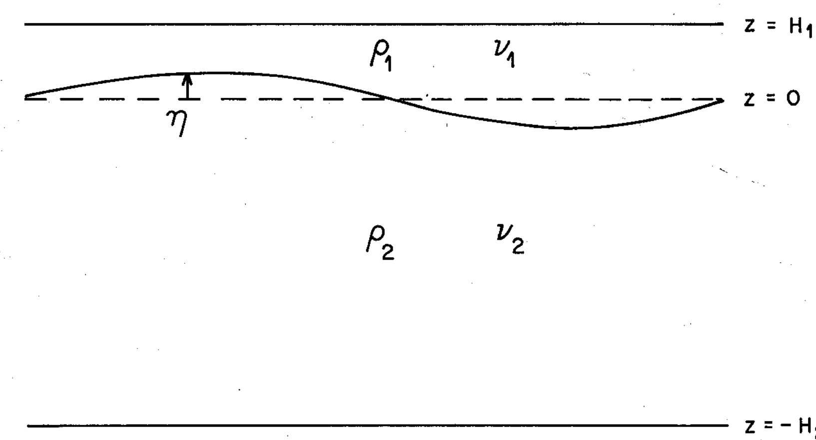

FIGURE 1 The two-layer geometry.

The general problem is outlined in Appendix A. Even for linear equations the derivation of a dispersion relation is far from simple. With vertical viscosity ν_V present there are no-slip and stress-matching boundary conditions to be satisfied. When rotation is included the appearance of Ekman layers further complicates the vertical structure. However, greater simplification can be gained if ν_V can be neglected. Some justification for this assumption comes from the comparison of results for $\nu_V=\nu_L$ and $\nu_V=0$ for a non-rotating system (ν_L is lateral eddy viscosity). As described at the end of Appendix A, omission of ν_V has negligible effect on growth rates for wavelengths up to several hundred metres. For large scales ($L \gg H_j$) we expect $\nu_V \ll \nu_L$, so the influence of ν_L should still dominate ν_V. Support for the neglect of Ekman pumping is given in Appendix C, where it is shown that addition of interface Ekman layers has little effect on σ_{max} and L_{max}. Hence vertical viscosity will be omitted in the following theory.

The linearised momentum equations are

$$u_t - fv = -\rho^{-1}\phi_x + \nu\nabla_L^2 u, \tag{2.1a}$$

$$v_t + fu = -\rho^{-1}\phi_y + \nu\nabla_L^2 v, \tag{2.1b}$$

$$w_t = -\rho^{-1}\phi_z + \nu\nabla_L^2 w, \tag{2.1c}$$

where f is the Coriolis parameter, $\phi=p+\rho gz$ (p=pressure), $\nu=\nu_L$ and $\nabla_L^2 = \partial^2/\partial x^2 + \partial^2/\partial y^2$. (Subscripts for separate layers will be omitted when equations apply to each layer.) The continuity equation is

$$u_x + v_y + w_z = 0. \tag{2.2}$$

It is useful to obtain equations in terms of vertical vorticity $\zeta = v_x - u_y$ and vertical velocity w. The horizontal divergence of (2.1) gives

$$w_{zt} + f\zeta = \rho^{-1}\nabla_L^2 \phi + \nu \nabla_L^2 w_z, \tag{2.3}$$

and the vertical component of the curl of (2.1) is

$$\zeta_t - f w_z = \nu \nabla_L^2 \zeta. \tag{2.4}$$

Another relation between ζ and w follows from $\nabla \times (\nabla \times (2.1))$:

$$\nabla^2 w_t + f\zeta_z = \nu \nabla_L^2 (\nabla^2 w). \tag{2.5}$$

Wavelike solutions are sought of the form

$$\left.\begin{matrix} w \\ \zeta \\ \phi \end{matrix}\right\} = \exp\left(i(kx+ly)\right)\exp(\sigma t)\left\{\begin{matrix} W(z) \\ Z(z) \\ P(z). \end{matrix}\right. \tag{2.6}$$

Then, (2.4) and (2.5) become

$$(\sigma + \nu K^2) Z = f W_z, \tag{2.7}$$

$$(\sigma + \nu K^2)(W_{zz} - K^2 W) = -f Z_z, \tag{2.8}$$

where $K^2 = k^2 + l^2$. Combining (2.3) and (2.4) gives, for later reference,

$$[\sigma + \nu K^2 + f^2/(\sigma + \nu K^2)] W_z = -\rho^{-1} K^2 P. \tag{2.9}$$

Eliminating Z from (2.7) and (2.8) leads to

$$[(\sigma + \nu K^2)^2 + f^2] W_{zz} - K^2 (\sigma + \nu K^2)^2 W = 0, \tag{2.10}$$

so we have

$$W = a \cosh \lambda z + b \sinh \lambda z, \tag{2.11}$$

with

$$\lambda^2 = K^2 (\sigma + \nu K^2)^2 / (f^2 + (\sigma + \nu K^2)^2).$$

Three boundary conditions on W are

$$\begin{aligned} W_1(H_1) &= 0 = W_2(-H_2), \\ W_1(0) &= W_2(0) \quad (= W_0, \text{ say}). \end{aligned} \tag{2.12}$$

(Note that the bottom boundary could be the ocean floor, or another (stable) interface with relatively large $\Delta\rho$ where w is negligible.)

The fourth relation needed to close the problem comes from pressure matching and kinematic conditions at the interface. From

$$\phi_2 - \phi_1 = g \Delta \rho \eta,$$

and

$$w = \eta_t,$$

we obtain

$$\sigma (P_2 - P_1) = g \Delta \rho W_0, \tag{2.13}$$

near $z = 0$. Using (2.9) to substitute for P_j then gives

$$\sigma \left[\frac{(\sigma + \nu_1 K^2)^2 + f^2}{\sigma + \nu_1 K^2} W_{1z} - \frac{(\sigma + \nu_2 K^2)^2 + f^2}{\sigma + \nu_2 K^2} W_{2z} \right] = g' K^2 W_0 \quad \text{at} \quad z = 0, \tag{2.14}$$

with $g' = g\Delta\rho/\rho$.

With boundary conditions (2.12) a non-trivial solution requires

$$\sigma \sum_{j=1}^{2} \frac{(\sigma + \nu_j K^2)^2 + f^2}{\sigma + \nu_j K^2} \frac{\lambda_j}{\tanh \lambda_j H_j} + g' K^2 = 0, \tag{2.15}$$

which is the dispersion relation we seek. A general property of this equation is that $\sigma > 0$ requires $\Delta\rho < 0$. As expected, only a density inversion ($\rho_1 > \rho_2$, $g' < 0$) can support a growing disturbance.

If rotational effects are ignored ($f \to 0$) then $\lambda_j = K$ and (2.15) reduces to the quadratic

$$\sigma \sum_{1}^{2} (\sigma + \nu_j K^2) \coth K H_j + K g' = 0. \tag{2.16}$$

For $g'<0$ there is one real positive and one real negative root, corresponding to purely growing and decaying disturbances.

3. SHORT AND LONG WAVE LIMITS, AND COMBINATIONS

When $K\to\infty$ (the short wave limit) both (2.15) and (2.16) reduce to

$$\sigma[2\sigma+(\nu_1+\nu_2)K^2]+g'K=0. \tag{3.1}$$

With $g'<0$ the growing root is

$$\sigma\sim -g'(\nu_1+\nu_2)^{-1}K^{-1}\to 0 \quad \text{as} \quad K\to\infty. \tag{3.2}$$

Not surprisingly, the short waves are independent of f and H_j.

For long waves ($L\gg H_j$), λ_j is small and the dispersion relation is, approximately,

$$\sigma\sum_1^2[\sigma+\nu_jK^2+f^2/(\sigma+\nu_jK^2)]/H_j+g'K^2=0. \tag{3.3}$$

When $f\neq 0$ the growth rate decreases very rapidly with K. We find

$$\sigma\sim -g'f^{-2}\nu_1H_1(1+\nu_1H_1/\nu_2H_2)^{-1}K^4\to 0 \quad \text{as} \quad K\to 0. \tag{3.4}$$

This limit depends on ν_j. For an inviscid system the long wave dispersion relation is

$$(\sigma/f)^2=(K/K_R)^2-1, \tag{3.5}$$

where

$$K_R^2=f^2(1+H_1/H_2)/(|g'|H_1).$$

In this special case wavelengths larger than the Rossby deformation wavelength $L_R=2\pi/K_R$ are stable! Addition of viscosity evidently destabilises the long waves. In Appendix B the dispersion relation (3.3) is derived from the shallow-water equations and an energy equation (an instructive alternative to the methods of the previous section), and the above behaviour is explained there in terms of energy balance.

When rotation is ignored ($f=0$) then growth rates decrease much more slowly with K:

$$\sigma\sim(-g'H_1)^{1/2}(1+H_1/H_2)^{-1/2}K. \tag{3.6a}$$

Note that this limit is independent of viscosity. Interestingly, if σ is scaled by some rotation rate f_0 then we can write (3.6a) as

$$\sigma/f_0\sim K/K_R. \tag{3.6b}$$

From the above limits we see that $\sigma\to 0$ for long and short waves, so there will be a maximum $\sigma_{\max}$ for some intermediate wavenumber $K_{\max}$. Rotation restricts the growth of long waves. However, we expect this effect to be unimportant with regard to $\sigma_{\max}$ if the fastest-growing waves have $L_{\max}<L_R$.

Results using the full dispersion relation are presented in the next section. Some simple and useful estimates of $\sigma_{\max}$ and $K_{\max}$ (denoted σ_{est} and K_{est}) can first be obtained by naively combining the limits, however. This method only yields order-of-magnitude approximations, but does reveal analytic behaviour. For simplicity we set $\nu_1=\nu_2=\nu$ and $H_1=H_2=H$ in the following relations.

For $f=0$ the short and long wave limits (3.2) and (3.6) intersect at

$$K_{\text{est}}=2^{-1/4}|g'|^{1/4}\nu^{-1/2}H^{-1/4}, \tag{3.7a}$$

with

$$\sigma_{\text{est}}=2^{-3/4}|g'|^{3/4}\nu^{-1/2}H^{1/4}. \tag{3.7b}$$

Due to the relatively weak dependence of σ on K this should be a reasonable estimate as long as rotation effects are minor, i.e. $\sigma_{\text{est}}\gtrsim f_0$. (Note that this implies $L_{\text{est}}\gtrsim L_R$, according to (3.6b).) If $L_{\text{est}}>L_R$ ($\sigma_{\text{est}}<f_0$) however, then the rapid long-wave attenuation of (3.4) may be more appropriate. This predicts

$$K_{\text{est}}=f^{2/5}\nu^{-2/5}H^{-1/5}, \tag{3.8a}$$

$$\sigma_{\text{est}}=\tfrac{1}{2}|g'|\nu^{-3/5}f^{-2/5}H^{1/5}. \tag{3.8b}$$

The dominant factor in the growth rate is the density over-burden $\Delta\rho$, as expected. For small $\Delta\rho$ growth is slow and the fastest-growing wavelength is independent of $\Delta\rho$, depending mainly on the effective viscosity. As $|\Delta\rho|$ increases σ_{est} increases and, with a transition from (3.8) to (3.7), L_{est} begins to decrease.

4. CALCULATIONS FOR OCEANIC SCALES

We are interested in the effect of rapidly cooling an ocean surface layer, and choose order-of-magnitude scales to simulate such an event. There is considerable uncertainty in these scales, so results for a wide range of values will be given. The only reliable parameter is f, and we use $f = 10^{-4}\,\mathrm{sec}^{-1}$. For the sinking event described by Stommel (1972), surface cooling rates in excess of 2000 gm cal cm^{-2} per day were estimated. With this figure as a guide, cooling the upper 10 metres gives $g' \approx -4 \times 10^{-5}\,\mathrm{m\,sec}^{-2}$, and cooling spread over 100 m has $g' \approx -4 \times 10^{-6}$. A representative figure $g' = -10^{-5}$ is chosen.

Estimation of ν_L is difficult. A lateral eddy viscosity $\nu = 1\,\mathrm{m}^2\,\mathrm{sec}^{-1}$ will be used as a standard. (This may be regarded as background turbulence with, for example, a mixing length of 10 m and velocity scale 0.1 m sec^{-1}.) In practice we expect ν to vary with wavelength, but this effect is ignored in the theory. Depth scales $H_1 = 100$ m, $H_2 = 1000$ m are used, to simulate sinking in a very weakly stratified upper ocean. Scales $H_1 = 10$ m, $H_2 = 100$ m are also considered, and may better represent initial stages of sinking.

Figure 2 shows growth rates (scaled by $f_0 = 10^{-4}\,\mathrm{sec}^{-1}$) as a function of

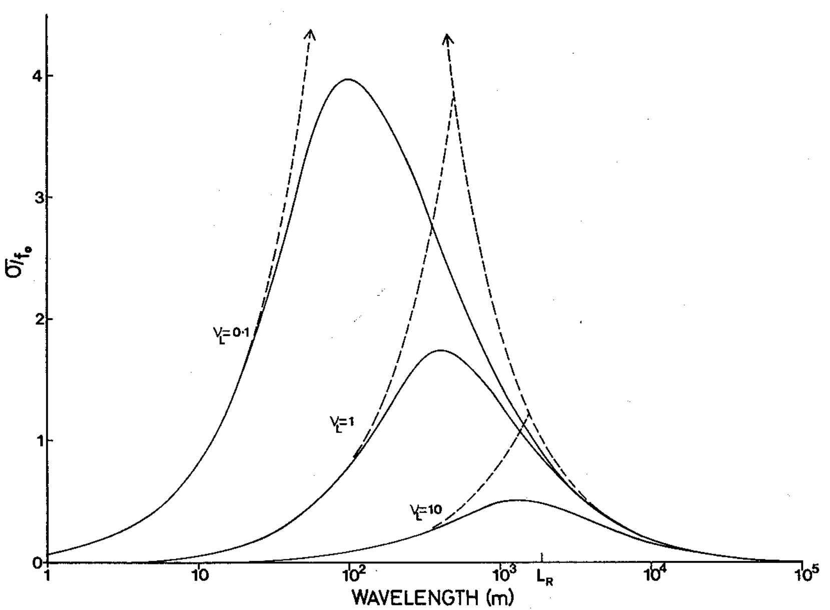

FIGURE 2 Growth rate (scaled by $f_0 = 10^{-4}\,\mathrm{sec}^{-1}$) as a function of wavelength for $g' = -10^{-5}\,\mathrm{m\,sec}^{-2}$, $H_1 = 100$ m, $H_2 = 1000$ m, $f = 0$, $\nu_V = 0$, ν_L (m^2 sec^{-1}) as indicated. Long and short wave limits are marked by dashed curves.

wavelength, with rotation neglected and $\nu_1 = \nu_2 = 0.1$, 1 and 10. There is a definite maximum, with the peak broadening and lowering with increasing ν. The e-folding time varies from 0.8 to 6 hours over the range considered, with $L_{\max}$ ranging from 100 m to 1200 m. The long and short wave dispersion relations are indicated by dashed lines in Figure 2, showing that they give reasonable order-of-magnitude estimates for $L_{\max} \gtrsim H$.

Values of $\sigma_{\max}$ and $L_{\max}$ for a wider range of ν and g' are given in Table Ia. These confirm the trends predicted by (3.7); $\sigma_{\max}$ depends more on g' than ν, vice-versa for $L_{\max}$.

Corresponding results with rotation included are shown in Figure 3 and Table Ib. Beyond the Rossby radius $L_R = 1890$ m, growth rates decrease

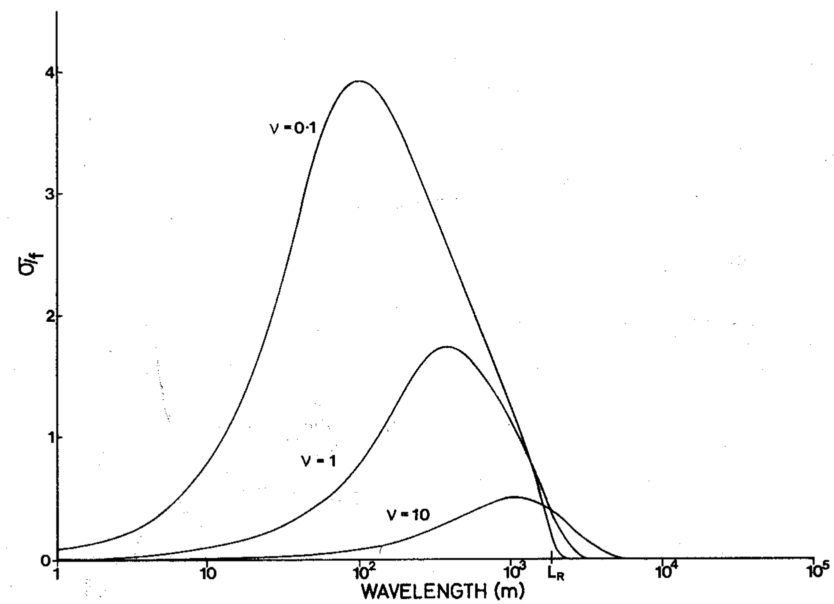

FIGURE 3 σ/f as a function of L for $g' = -10^{-5}\,\mathrm{m\,sec}^{-2}$, $H_1 = 100$ m, $H_2 = 1000$ m, $f = 10^{-4}\,\mathrm{sec}^{-1}$, $\nu_V = 0$, ν_L (m^2 sec^{-1}) as indicated.

rapidly, particularly when viscosity is small. The maxima in Figure 3 have $L_{\max} < L_R$ however, and rotation has little effect on $\sigma_{\max}$, as can be seen by comparing Tables Ia and Ib.

When $\Delta\rho$ is relatively small growth rates are lower and rotation has more effect. Growth rates for $g' = -10^{-6}$, with and without rotation, are shown in Figure 4 for $\nu_1 = \nu_2 = 1$. Inclusion of f changes $L_{\max}$ from greater to less than L_R and decreases $\sigma_{\max}$ by about 20%. The short and long

TABLE Ia

Maximum growth rates σ_{max}/f_0 and wavelengths L_{max} for $H_1 = 100$ m, $H_2 = 1000$ m, neglecting rotation

g' \ ν	0.01	0.1	1	10	100
-10^{-3}			39 100 m		
-10^{-4}			8.5 220 m		
-10^{-5}	8.6 20 m	4.0 100 m	1.8 400 m	0.52 1300 m	0.082 4500 m
-10^{-6}			0.33 740 m		

TABLE Ib

As for Table Ia, including $f = 10^{-4}$ sec^{-1}

g' \ ν	0.01	0.1	1	10	100	L_R
-10^{-3}			39 100 m			18900 m
-10^{-4}			8.5 200 m			6000 m
-10^{-5}	8.5 20 m	4.0 100 m	1.7 360 m	0.49 1000 m	0.076 2800 m	1890 m
-10^{-6}			0.27 480 m			600 m

wave limits with rotation are shown as dashed lines in Figure 4. The long wave approximation is strongly dependent on L so σ_{max} is greatly overestimated, but a reasonable value of L_{max} is defined.

The above results use $\nu_1 = \nu_2$. In the lower, deeper layer ν_2 may well be comparatively small. To see how this affects the system, growth rates for $\nu_2 = 1$ and 0.01 (with $\nu_1 = 1$) are compared in Figure 5. Only a small change is found, much less than that produced by reducing ν_1 and ν_2 to 0.1 for example, so a good estimate of the largest ν is far more important than details of viscosity variability.

Table II shows σ_{max} and L_{max} for the smaller depths $H_1 = 10$ m and $H_2 = 100$ m, and can be compared with Table I. For relatively large g' and small ν the tenfold decrease in vertical scale reduces σ_{max} and L_{max} only slightly. The effect increases as $|g'|$ increases and ν decreases, however. For the standard case ($g' = -10^{-5}$, $\nu = 1$) σ_{max} is approximately halved by the scale change.

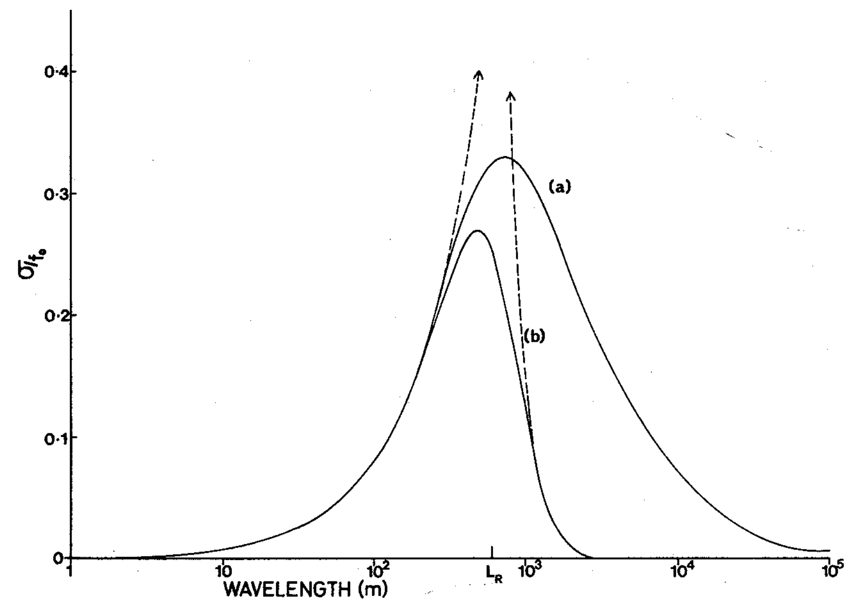

FIGURE 4 σ/f_0 as a function of L for $g' = -10^{-6}$ sec^{-2}. $H_1 = 100$ m, $H_2 = 1000$ m, $\nu_V = 0$, $\nu_L = 1$ (a) without rotation, $f = 0$ (b) $f = 10^{-4}$ sec^{-1}.

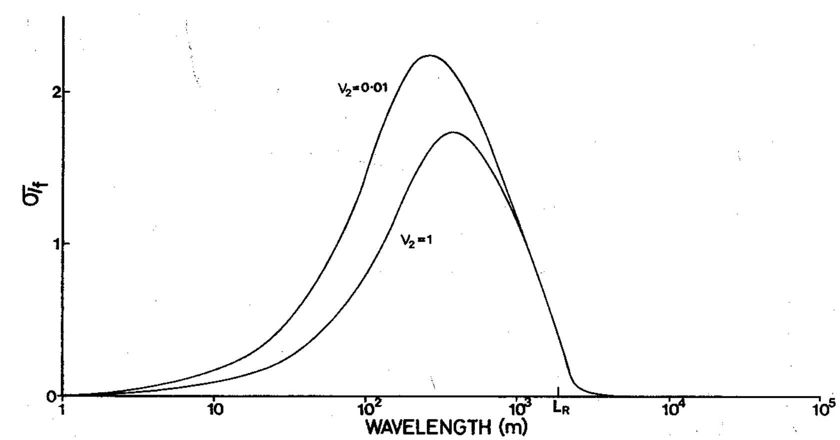

FIGURE 5 σ/f as a function of L for $g' = -10^{-5}$ m sec^{-1}, $H_1 = 100$ m, $H_2 = 1000$ m, $\nu_V = 0$, $\nu_1 = 1$ m^2 sec^{-1}, ν_2 as indicated.

TABLE IIa

Maximum growth rates σ_{max}/f_0 and wavelengths L_{max} for $H_1 = 10$ m, $H_2 = 100$ m, neglecting rotation.

g' \ ν	0.1	1	10
-10^{-4}		5.3 120 m	
-10^{-5}	3.3 70 m	0.71 250 m	0.088 800 m
-10^{-6}		0.082 500 m	

TABLE IIb

As for Table IIa, including $f = 10^{-4}$.

g' \ ν	0.1	1	10	L_R
-10^{-4}		5.2 130 m		1890 m
-10^{-5}	3.3 70 m	0.69 250 m	0.087 600 m	600 m
-10^{-6}		0.076 300 m		189 m

5. DISCUSSION

The scenario we envisage involves a large-scale rapid surface cooling producing a small density inversion. When g' and H_1 are small initially, the fastest-growing length scale is large, $\sigma < f$, and rotation effects inhibit sinking. Continued cooling may then maintain or increase the density overburden, effectively increasing $|g'|$ and H_1. This process decreases L_{max} and increases σ until convection cells are established that counterbalance the surface cooling. If $g' = -10^{-5}$ and $\nu = 1$ are representative values, then the results of Section 4 lead us to expect overturning on length scales of about 500 m. The main point of this essentially qualitative description is that the response to widespread surface cooling is sinking in relatively small cells.

One might further postulate that seed cells occur at preferred sites due to local stratification details, and may be rather widely spaced. Alternatively, several cells may combine in advanced stages of sinking to form a supercell—unfortunately the very simple model we have described cannot address such questions.

Other aspects not included in the model are the overturning time and depth and entrainment effects. The linear theory only estimates initial growth rates for small perturbations. If several e-folding times are needed for convective overturning, then a large density anomaly can build up, and may sink to great depths on a small length scale. If the turnover time is small, however, then $\Delta\rho$ is relatively small and sinking is less dramatic.

Acknowledgements

This work was initiated while both authors were participating in the Advanced Study Program at the National Centre for Atmospheric Research. The National Center for Atmospheric Research is sponsored by the National Science Foundation.

References

Chandrasekhar, S., *Hydrodynamic and Hydromagnetic Stability*. Oxford: Clarendon Press (1961).

Hide, R., "The character of the equilibrium of a heavy, viscous, incompressible, rotating fluid of variable density. I, General theory; II, Two special cases," *Q. J. Mech. Appl. Math.* **9**, 22–50 (1956).

MEDOC Group: H. Lacombe, P. Tchernia, M. Ribet, J. Bonnot, R. Frassetto, J. C. Swallow, A. R. Miller and H. Stommel, "Observation of the formation of deep water in the Mediterranean Sea," *Nature* **227**, 1037–1040 (1969).

Stommel, H., "Deep winter-time convection in the western Mediterranean Sea," *Studies in Phys. Ocean.* **2**, 207–218 (1972).

Appendix A
GENERAL LINEAR THEORY

For simplicity we assume $\nu_V = \nu_L$ in this section. Equations (2.3) to (2.5) relating ζ and w are then slightly modified by replacing ∇_L^2 by ∇^2. As in Section 2, wavelike disturbances are assumed and Z is eliminated to get an ordinary differential equation for W. In place of the second-order Eq. (2.10), the following sixth-order equation is obtained:

$$\left[\nu\frac{d^2}{dz^2} - (\sigma + \nu K^2)\right]^2\left(\frac{d^2}{dz^2} - K^2\right)W + f^2 W_{zz} = 0. \tag{A1}$$

For this two-layer system, twelve boundary conditions are needed. At the flat stress-free upper surface

$$w = u_z = v_z = 0,$$

which implies

$$W_1 = W_{1zz} = Z_{1z} = 0 \quad \text{at} \quad z = H_1. \tag{A2}$$

No-slip conditions at the bottom boundary give

$$W_2 = W_{2z} = Z_2 = 0 \quad \text{at} \quad z = -H_2. \tag{A3}$$

At the interface, velocity matching requires

$$W_1 = W_2, \quad W_{1z} = W_{2z}, \quad Z_1 = Z_2. \tag{A4}$$

Tangential stress matching gives

$$\mu_1(u_{1z} + w_{1x}) = \mu_2(u_{2z} + w_{2x}),$$

$$\mu_1(v_{1z} + w_{1y}) = \mu_2(v_{2z} + w_{2y}),$$

where $\mu_j = \rho_j \nu_j$. In terms of W and Z we find

$$\mu_1(W_{1zz} + K^2 W_1) = \mu_2(W_{2zz} + K^2 W_2),$$
$$\mu_1 Z_{1z} = \mu_2 Z_{2z}. \tag{A5}$$

The twelfth condition is obtained by normal stress matching, analogous to the pressure matching in Section 2.

The algebra required for a general dispersion relation is too cumbersome to be worth attempting for our purpose. As a compromise we consider the effect of ν_V on the non-rotating system. In this case the flow is irrotational ($Z \equiv 0$) and a fourth-order equation for W is obtained. For each layer

$$W = a \cosh Kz + b \sinh Kz + c \cosh \alpha z + d \sinh \alpha z,$$

where

$$\alpha^2 = K^2(1 + \sigma/\nu K^2).$$

For further simplification $\nu_1 = \nu_2$ is assumed. The dispersion relation is still complicated, so only the result for one case is presented. Growth rates as a function of wavelength are given in Figure 6 for $H_1 = 100$, $H_2 = 1000$, $g' = -10^{-5}$, $\nu_L = 1$. The curves with $\nu_V = 0$ and $\nu_V = 1$ are almost identical for $L \gtrsim 300\,m$. At longer wavelengths, growth rates are slightly lower when $\nu_V = 1$.

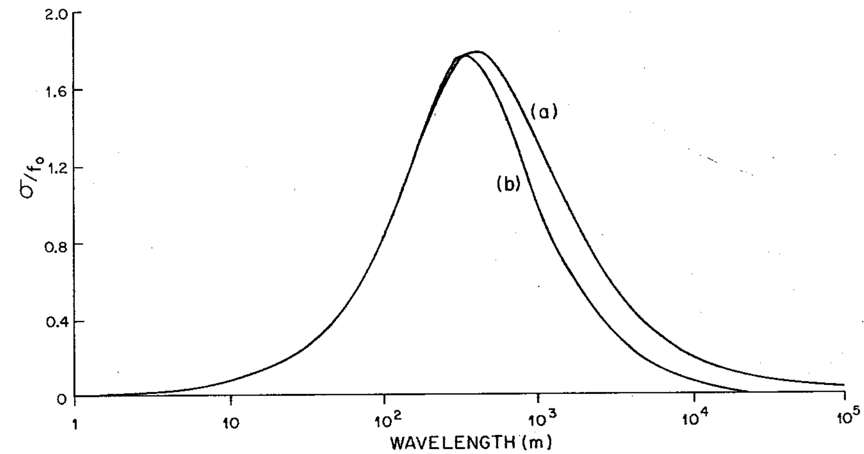

FIGURE 6 σ/f_0 as a function of L for $g' = -10^{-}$ m sec^{-2}, $H_1 = 100$ m, $H_2 = 1000$ m, $\nu_L = 1$ m^2 sec^{-1}, neglecting rotation. (a) $\nu_V = 0$ (b) $\nu_V = \nu_L$.

Appendix B

SHALLOW-WATER EQUATIONS

The momentum Eqs. (2.1a, b) apply with u and v independent of depth. Vertical velocity is a linear function of z, and continuity requires

$$u_{1x} + v_{1y} - \eta_t / H_1 = 0, \tag{B1a}$$

$$u_{2x} + v_{2y} + \eta_t / H_2 = 0. \tag{B1b}$$

The vorticity Eqs. (2.4) become

$$\zeta_{1t} + f\eta_t / H_1 = \nu_1 \nabla_L^2 \zeta_1, \tag{B2a}$$

$$\zeta_{2t} - f\eta_t / H_2 = \nu_2 \nabla_L^2 \zeta_2. \tag{B2b}$$

Wavelike solutions are

$$\eta = A \exp(i\mathbf{k} \cdot \mathbf{x}) \exp(\sigma t), \quad \mathbf{u}_j = \mathbf{U}_j \exp(i\mathbf{k} \cdot \mathbf{x}) \exp(\sigma t). \tag{B3}$$

The potential energy averaged over a wavelength is

$$\overline{PE} = \tfrac{1}{4} g' \rho |A|^2 \exp(2\sigma t). \tag{B4}$$

Expressions for $\mathbf{U}_j$ in terms of A can be easily obtained from (B1) and

(B2). Kinetic energy is then given by

$$\overline{KE_j}=\tfrac{1}{4}\rho|A|^2\left(\sigma^2+f^2\frac{\sigma^2}{(\sigma+\nu_jK^2)^2}\right)\frac{1}{H_jK^2}\exp(2\sigma t). \tag{B5}$$

When averaged over a wavelength the energy equation is

$$\frac{d\overline{E}}{dt}=\frac{d}{dt}(\overline{KE_1}+\overline{KE_2}+\overline{PE})=-\nu_1K^2\overline{KE_1}-\nu_2K^2\overline{KE_2}, \tag{B6}$$

where $\overline{E}=\overline{KE_1}+\overline{KE_2}+\overline{PE}$ is total energy.

Substituting (B4) and (B5) into (B6) gives the shallow-water dispersion relation

$$\sum_j(\sigma+\nu_jK^2)\left(\sigma^2+f^2\frac{\sigma^2}{(\sigma+\nu_jK^2)^2}\right)\frac{1}{H_jK^2}+\sigma g'=0, \tag{B7}$$

which is equivalent to (3.3).

When $\Delta\rho<0$ potential energy decreases as the interface displacement increases. Though total energy must decrease due to dissipation effects, kinetic energy can increase as long as the increase is less than (or equal to, if inviscid) the potential energy change. For very long waves only very small growth rates can be accommodated. The effect of rotation is to add to the KE produced by interface displacement, by vortex stretching of the background vorticity f, so lower growth rates are required. For the inviscid case, KE production exceeds PE reduction when $L>L_R$. Note that lateral viscosity attenuates the influence of rotation in each layer by effectively replacing f by $f\sigma/(\sigma+\nu_jK^2)$ in (B7).

The shallow-water result does not apply as $K\to\infty$. Equation (B7) predicts

$$\sigma\to-g'/(\nu_1/H_1+\nu_2/H_2)\quad\text{as}\quad K\to\infty. \tag{B8}$$

This is a maximum with respect to K. Shallow-water theory does not define a fastest-growing wave at finite wavelength because the short-wave effects that decrease σ to zero as $K\to\infty$ are omitted. However, (B8) does give a useful upper bound for the general theory. It confirms the intuitive feeling that σ increases as $|\Delta\rho|$ increases, ν_j decreases and H_j increases.

Appendix C

INCLUSION OF INTERFACE EKMAN LAYERS

To obtain a crude estimate of vertical viscosity effects on a rotating system we can add interface Ekman layers. We assume that such layers are established instantly, and that they have depth $H_E\ll H_j$. [Ekman layer depth is $(2\nu_V/f)^{1/2}$, so the second assumption is good for $\nu_V\lesssim10^{-2}\,\text{m}^2\,\text{sec}^{-1}$, if $H_j\gtrsim10^2$ m. The first assumption should overestimate the influence of ν_V.] The effect is to add a vertical velocity

$$W_E=\tfrac{1}{4}H_E(Z_1-Z_2) \tag{C1}$$

at the interface $z=0$, which changes the condition (2.13) to

$$\sigma(P_2-P_1)=g\Delta\rho(W_0-W_E). \tag{C2}$$

Consequently the term $g'K^2$ in the dispersion relation (2.15) becomes

$$g'K^2\left\{1+\tfrac{1}{4}H_E\sum_1^2\frac{f}{(\sigma+\nu_jK^2}\frac{\lambda_j}{\tanh\lambda_jH_j}\right\}. \tag{C3}$$

For $\sigma>0$ the term $\{\}$ is greater than 1, so vertical viscosity in this form effectively increases $|g'|$ and hence increases growth rate. (This result is similar to the destabilising effect of ν_L on long waves found earlier.)

The long-wave approximation simplifies (C3) to

$$g'K^2\left\{1+\tfrac{1}{4}\sum_1^2\frac{f}{\sigma+\nu_jK^2}\frac{H_E}{H_j}\right\}. \tag{C4}$$

With $H_E\ll H_j$ and K small we see that the Ekman effect is small unless $f\gg\sigma$. Numerical calculations with $|g'|=10^{-6}$ and $\nu_L=1$ show an increase of about 2% in $\sigma_{\max}$ when $H_E=10$ m is added.